Available online at www.sciencedirect.com

SciVerse ScienceDirect

Ceramics International 38 (2012) 3167–3174

CERAMICS INTERNATIONAL

www.elsevier.com/locate/ceramint

The adsorption feature and photocatalytic oxidation activity of $K_{1-2x}M_xTiNbO_5$ (M = Mn, Ni) for methyl mercaptan in methane

Weimeng Cai, Guohui Lu, Jie He *, Yunxiang Lan

School of Chemical Engineering, Anhui University of Science and Technology, Huainan 232001, PR China

Received 19 October 2011; received in revised form 9 November 2011; accepted 12 December 2011
Available online 19 December 2011

Abstract

The novel photocatalytic ceramics material $K_{1-2x}M_xTiNbO_5$ (M = Mn, Ni) were prepared through Mn^{2+} and Ni^{2+} ion-exchange of $KTiNbO_5$, which was synthesized by a hydrothermal method. The influence of the ion-exchange process on the structure and morphology of prepared ceramics material were investigated by such physicochemical methods as powder X-ray diffraction (XRD), scanning electron microscope (SEM), high-resolution transmission electron microscope (HRTEM), UV–visible diffuse reflectance spectroscopy (UV–vis DRS) and Fourier-transform infrared (FT-IR) microscopy. The adsorption and photocatalytic oxidation of methyl mercaptan (MM) in methane were used to evaluate the catalytic performance of different constitutes. The results revealed that $K_{1-2x}Ni_xTiNbO_5$ exhibited better adsorption and photocatalytic oxidation activity for MM in methane under both visible and UV light radiation. While the photocatalytic oxidation activity of $K_{1-2x}Mn_xTiNbO_5$ is similar to that of $K_{1-2x}Ni_xTiNbO_5$, however it has little adsorption activity for MM in dynamic state.

Keywords: Titanoniobate; Ion exchange; Methyl mercaptan; Adsorption; Photocatalytic oxidation

1. Introduction

Clean energy has been accepted and promoted by more and more countries to reduce pollution and protect environment. The clean technology of hydrocarbon fuels like natural gas, liquefied petroleum gas and gasoline has been one of important research themes, such as the desulfurization and denitrification technology. Especially, sulfides not only could be oxidated to SO_2, which eventually becomes H_2SO_4 and leads to acid rain, but also could do harm to anode catalysts in fuel cell using hydrocarbon. Therefore, how to reduce the content of sulfur compounds in hydrocarbon fuels to the lowest level has become a significant issue in current researches and studies.

Currently, the photocatalytic oxidation technology has been a promising method to decompose many odorous compounds [1–5] such as mercaptans, sulfides, and hydrogen sulfide. Of all the photocatalysts, inorganic host materials with the unique layered structure have become popular not only for cationic exchange or organic intercalation [6,7], but also for the generation of new properties such as photoluminescence [8,9], and their distinctive photochemical and semiconductor properties in the field of photocatalysis [10–18]. Layered titanoniobates, which are consisted of Ti, Nb host layers, are regarded as typical photocatalysts for water photolysis into H_2 and O_2 under ultraviolet light radiation [19,20]. $KTiNbO_5$ is an important layered compound, as shown in Fig. 1, it is consists of corner- and edge-shared NbO_6 and TiO_6 octahedral units, which form a two-dimensional layered (nano-sheet) structure [21]. There is negatively charged on each sheet, and K^+ ions are located between sheets to compensate the negative charge of the layers. The photocatalytic reactivity of titanoniobates strongly depends on the combination between the host layers and the guest cations. Hosogi and co-workers have reported the catalytic performance and the structure characterization of layered titanoniobates and niobates, such as $KTiNbO_5$ and $K_4Nb_6O_{17}$, prepared by Sn^{2+} ion-exchange. The result indicated that the exchanged samples had absorption bands in visible light region and had highly activity for H_2 evolution from an aqueous methanol solution [22]. Jung et al. reported that the layered compound intercalated with Fe_2O_3 nanoparticles absorbed visible light due to Fe_2O_3 [16]. However, some key problems, such as the influence of exchanged metal

* Corresponding author. Tel.: +86 554 6668520; fax: +86 554 6668900.
E-mail address: jhe@aust.edu.cn (J. He).

0272-8842/$36.00
doi:10.1016/j.ceramint.2011.12.020

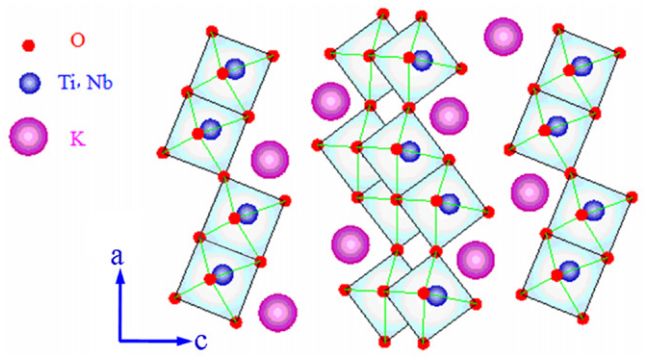

Fig. 1. Schematic of $KTiNbO_5$ structure. Squares represent the TiO_6 (and NbO_6) octahedral, and circles indicate the exchangeable cation K^+ in the interlayer.

ions on the structure of catalysts, adsorption and reaction mechanisms, are still ambiguous.

In the present work, the layered ceramics materials $K_{1-2x}M_xTiNbO_5$ (M = Mn, Ni) were prepared from host $KTiNbO_5$ by ion exchange with Mn^{2+} and Ni^{2+} respectively. Then their microstructure, morphology and optical absorbance property were investigated by means of XRD, SEM, HRTEM, FT-IR spectroscopy, and UV–vis DRS. Meantime, FT-IR spectroscopy was also employed to investigate the adsorption species and photocatalytic oxidization species on the samples as-prepared under visible light or ultra light radiation for MM in methane.

2. Experimental

2.1. Preparation of samples

The starting reagents used in the hydrothermal synthesis were titanium hydroxide powder (prepared by hydrolysis of tetrabutyl titanate, 98.5%), Nb_2O_5 fine powder (99.95%) and potassium hydroxide (85%). First, stoichiometric amounts of Nb_2O_5, $Ti(OH)_4$ and 50 ml KOH aqueous solution (concentration: 1 mol L^{-1}) were mixed and stirred until it become a white slurry. Then, the slurry was put into a 50 mL polytetrafluoroethylene (PTEE)-lined autoclave. The hydrothermal reaction was carried out at 508 K for 72 h with autogenous pressure inside the autoclave. Upon completion of the reaction, the PTEE tube containing product was taken out, and the white precipitates were filtrated and washed with distilled water, and then dried at 353 K for 12 h. $K_{1-2x}M_xTiNbO_5$ (M = Mn, Ni) were prepared by ion exchange with Mn^{2+} or Ni^{2+}. The ion-exchange reaction was carried out by adding 1.5 g $KTiNbO_5$ powder to 50 mL 2 mol L^{-1} $Mn(NO_3)_2$ (or $Ni(NO_3)_2$) aqueous solution and stirred at 333 K for 48 h, with the replacement of fresh 50 ml of 2 mol L^{-1} $Mn(NO_3)_2$ (or $Ni(NO_3)_2$) aqueous solution every 8 h. Subsequently, the obtained powder was washed with deionized water and dried at 353 K for 12 h. As a result of the whole procedure, $K_{1-2x}Mn_xTiNbO_5$ and $K_{1-2x}Ni_xTiNbO_5$ were obtained respectively. Additionally, all chemicals used in the experiment were directly used without further purification and deionized water was also used in the whole experiment.

2.2. Characterization

In this study, the crystal phases of the resulting powders were determined by powder X-ray diffraction (XRD) performed on a XD-3 diffractometer (Beijing Purkinje General Instrument Co. Ltd.) with a curved graphite monochromator operating at 40 kV and 30 mA, using Cu$K\alpha$ radiation (λ = 0.15418 nm). The morphologies and structure of the samples as-prepared were observed by a Hitachi TM-1000 scanning electron microscope (SEM) (KYKY Technology Development Ltd.) with an acceleration voltage of 25 kV, and JEOL 2010 high-resolution transmission electron microscopy (HRTEM) (JEOL Ltd.) with an acceleration voltage of 200 kV. The optical properties of the samples as-prepared were analyzed with a TU-1901 UV–visible diffuse reflectance spectrometer (Beijing Purkinje General Instrument Co. Ltd.) with an integrating sphere in the wavelength range of 250–800 nm, and $BaSO_4$ as a reference. Fourier-transform Infrared (FT-IR) spectra of the samples dispersed in KBr were collected on a Bruker Vector 33 FT-IR spectrophotometer (DTGS detector) with a resolution of 4 cm^{-1}.

2.3. Adsorption and photocatalytic oxidation

Adsorption feature and photocatalytic oxidation activity of the samples as-prepared for methyl mercaptan (MM) in methane were evaluated at room temperature using a fixed bed reactor as shown in Fig. 2. 50 mg sample was placed at the center of the reactor, which consists of quartz U-tube, and filled

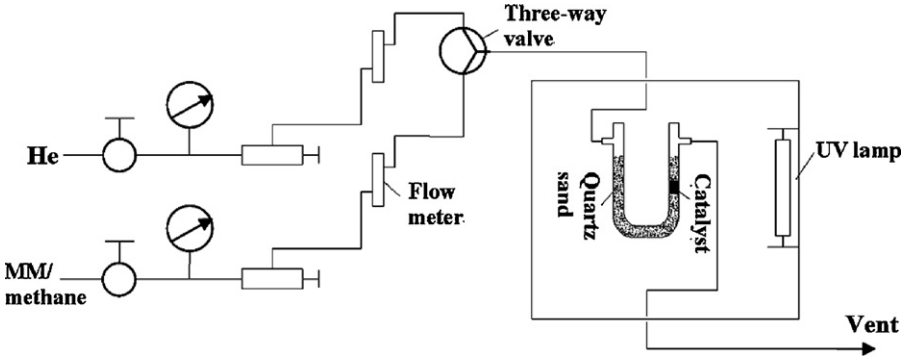

Fig. 2. Schematics flowchart of desulphurization experimental system.

with quartz sand on the both ends of the sample. In this experimental system, there are two passages of gas connecting to the reactor: one passage is for MM-loading methane (the concentration of MM was 19.6 ppm), and the other is for He (the purity was higher than 99.99%). The samples were purged for 1 h with He (flow rate of 20 ml min^{-1}), then the MM-loading methane (gas hourly space velocity 28,309 h^{-1}) was switched by a three-way valve to the line for adsorption at room temperature for 1 h. The photocatalytic oxidization activity of the catalysts as-prepared for oxidizing MM in methane was evaluated using the above-mentioned reactor under UV radiation, which was generated from a 300 W high-pressure mercury lamp (GGZ-300, Shanghai Yaming Lighting Co., Ltd.) with wavelength centered at 365 nm for 1 h. The condition of the passage gas for photocatalytic reaction was similar to that of adsorption experiment. The surface species on the samples after adsorption and photocatalytic oxidization were determined by FT-IR spectroscopy.

3. Results and discussion

3.1. X-ray diffraction

Powder X-ray diffraction (XRD) has been used to study the effect of ion exchange on the microstructure of the samples as-prepared, and the corresponding results have been shown in Fig. 3. According to Fig. 3(a), all the diffraction peaks can be indexed as the orthorhombic $KTiNbO_5$ phase (JCPDS 71-1747), which indicated that the obtained powder has the pure structure of $KTiNbO_5$. Especially, the diffraction peak at $2\theta = 9.20^\circ$ corresponds to plane (0 0 2), and the d value for the plane (0 0 2) was 0.960 nm according to the Bragg equation $\lambda = 2d\sin\theta$, which consistent with the lamellar spacing of the $KTiNbO_5$. After ion-exchanged, the diffraction peak corresponding to the plane (0 0 2) of $K_{1-2x}Mn_xTiNbO_5$ and $K_{1-2x}Ni_xTiNbO_5$ are observed at a lower angle ($2\theta = 8.56$ and 7.88° respectively), and their corresponding d-spacing values are 1.013 and 1.122 nm, respectively. The main reason of the differences in the d-spacing values results from the difference in the aqueous ionic radii of the cations ($r(Ni^{2+}) > r(Mn^{2+}) > r(K^+)$) occupying the interlayer sites of the sheets. According to Fig. 3(b) and (c), the lamellar structure of the host was well retained after ion-exchanged. Moreover, Fig. 3(b) and (c) also illustrated that the diffraction intensity of exchanged samples decreased compared with that of the host lattice ($KTiNbO_5$), indicating the periodic lamellar structure of the host compound could be partially destroyed by ion-exchange process. However, the presence of diffraction peaks indexed to the in-plane diffraction, such as (2 0 0) plane (ca. $2\theta = 27.8^\circ$) in the patterns of $K_{1-2x}Mn_xTiNbO_5$ and $K_{1-2x}Ni_xTiNbO_5$, indicates that the two-dimensional structure is preserved after ion-exchange.

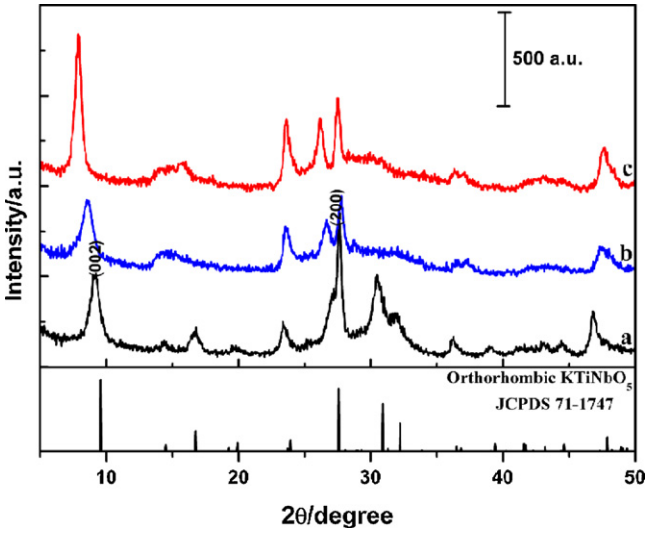

Fig. 3. XRD patterns of the samples as-prepared: (a) $KTiNbO_5$; (b) $K_{1-2x}Mn_xTiNbO_5$; and (c) $K_{1-2x}Ni_xTiNbO_5$.

3.2. Scanning electron microscopy and high resolution transmission electron microscopy

The SEM images of $KTiNbO_5$-based samples are illustrated in Fig. 4(a)–(d). Fig. 4(a) exhibits that the host $KTiNbO_5$ is composed of a number of nano-plates with 3D flower-like clusters. The high-magnification image demonstrated that the microstructure of single flower-like consisted of many intercrossed $KTiNbO_5$ nanoflakelets, and each flakelet showed fringes of regular interval of ca. 50 nm. This morphology result also demonstrated the reason of the as-prepared sample with higher BET surface area comparing with the sample synthesized by solid-state reaction. In the present research, Nb_2O_5 and $Ti(OH)_4$ reacted with KOH to produce $KTiNbO_5$ nuclei during the hydrothermal synthesis process. The process of growth was anisotropic as shown in the Fig. 4(a). Once the plate-like particles were produced, and they would simultaneously aggregate to form flower-like colonies. These plate-like particles had different sizes, which could be induced through the random nucleation and growth processes. After ion-exchange with Mn^{2+} or Ni^{2+}, Fig. 4(c) and (d) reveals that the flower-liked morphologies were completely deteriorated, and had less distinct edges. Although they still maintained layered structures as shown in XRD patterns, there was no regular stacking of platelets, especially for $K_{1-2x}Mn_xTiNbO_5$. These observations could explain the reduced peak intensity (0 0 2) of ion-exchanged samples in Fig. 3, which were consistent with ones measured by XRD.

To investigate the detailed structure of $KTiNbO_5$ nano-plates produced by the hydrothermal reaction, the samples as-prepared were examined by high-resolution transmission electron microscopy (HRTEM). Fig. 5(a)–(d) showed the images of three different samples. Fig. 5(a) revealed the regularly lamellar structure of $KTiNbO_5$ as-prepared. Fig. 5(b) showed the lattice fringe image of a $KTiNbO_5$ particle, and the basal spacing of 0.930 nm coincided with the d-spacing of the (0 0 2) lattice plane of $KTiNbO_5$ determined by XRD method. After ion-exchange with aqueous Mn^{2+} and Ni^{2+}, the HRTEM images showed that all these modified samples maintained a very good nano-sheet structure and the original in-plane structure. Such results would be also in agreement with the XRD results. Therefore, the host $KTiNbO_5$ prepared by

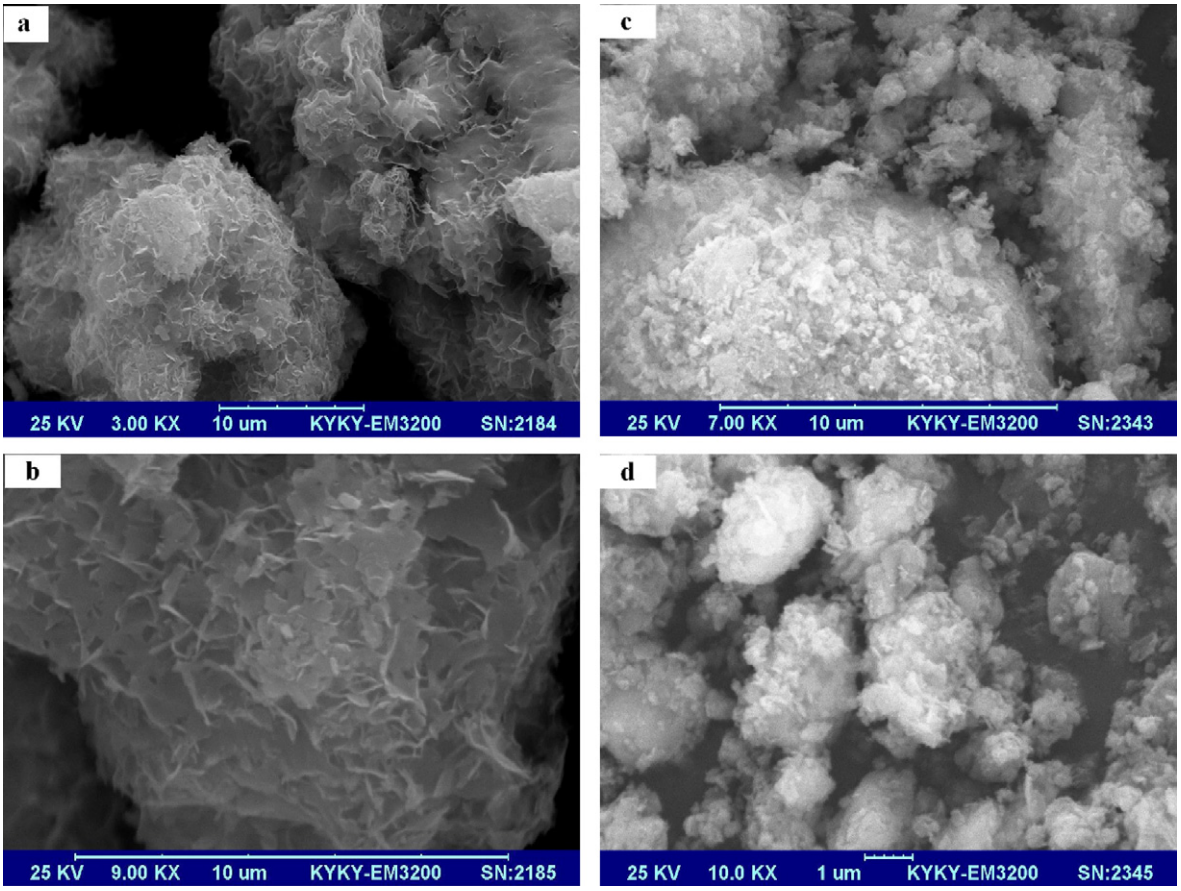

Fig. 4. SEM images of the $K_{1-2x}M_xTiNbO_5$ samples as-prepared: (a) and (b) $KTiNbO_5$; (c) $K_{1-2x}Mn_xTiNbO_5$; and (d) $K_{1-2x}Ni_xTiNbO_5$.

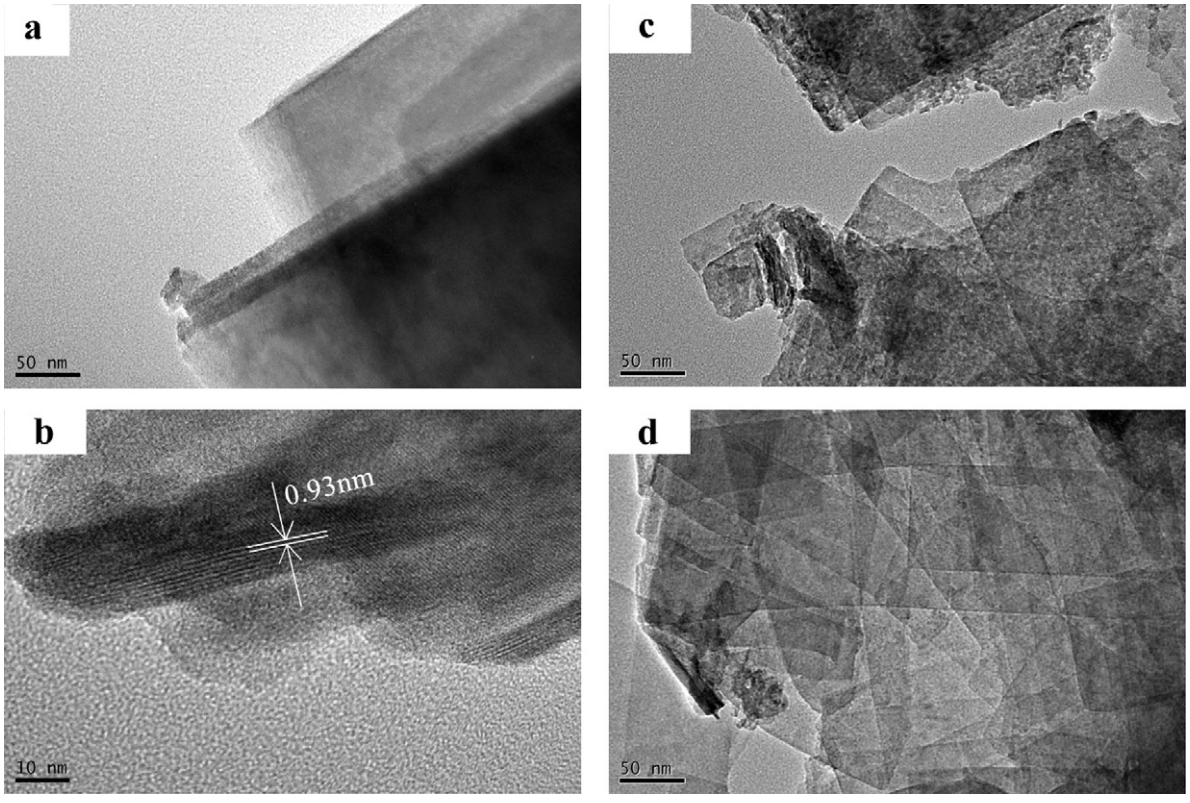

Fig. 5. HRTEM photographs of the samples as-prepared: (a) and (b) $KTiNbO_5$; (c) $K_{1-2x}Mn_xTiNbO_5$; and (d) $K_{1-2x}Ni_xTiNbO_5$.

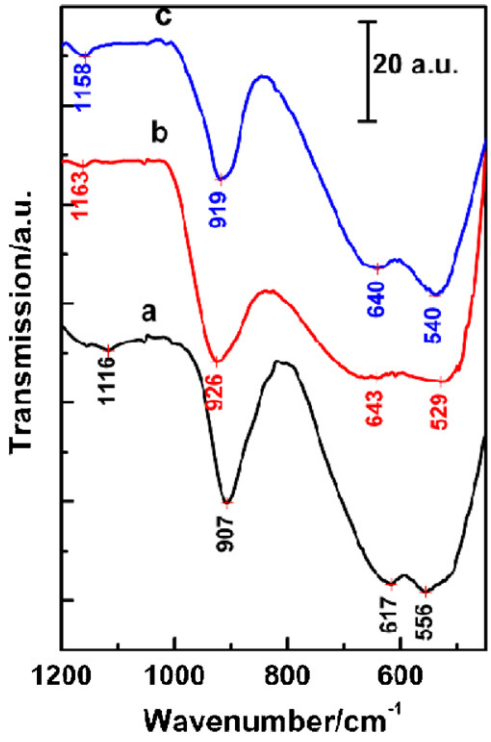

Fig. 6. FT-IR spectra of the samples as-prepared: (a) $KTiNbO_5$; (b) $K_{1-2x}Mn_xTiNbO_5$; and (c) $K_{1-2x}Ni_xTiNbO_5$.

hydrothermal reaction has been partly exfoliated and swollen during ion-exchange process.

3.3. FT-IR spectra

Fig. 6 shows the FT-IR spectra of the samples. For the host $KTiNbO_5$, the bands at 907 cm^{-1} and 556 cm^{-1} could be assigned to the stretching vibrations of the terminal Nb–O bond and the Nb–O–Nb bridging bond, respectively [23]. The band at 617 cm^{-1} arised from the stretching vibration of Ti–O–Ti bond [10,24–27].

In the case of $K_{1-2x}Mn_xTiNbO_5$ and $K_{1-2x}Ni_xTiNbO_5$, the band peak at 907 cm^{-1}, which is assigned to the stretching vibration of terminal Nb–O bond, produced a blue shift to 922 cm^{-1} and 916 cm^{-1}, respectively. This result could be induced by the bond strength changed due to the bigger Mn^{2+} and Ni^{2+} ions replacement. In other words, the band shifts could arise from the interaction between interlayer metal ions and terminal Nb–O bond. Compared with K^+ ion, aqueous Mn^{2+} and Ni^{2+} ions had stronger static electrostatic field, which would result in a stronger interactions between the cations and Nb–O bonds. Compared with $K_{1-2x}Mn_xTiNbO_5$, $K_{1-2x}Ni_xTiNbO_5$ has a smaller shift, because aqueous Ni^{2+} ion have a larger ionic radius and a weaker electrostatic field. Similarly, the vibration of Nb–O–Nb bond and Ti–O–Ti bond is also affected by interlayer exchanged cations.

As we know, the interlayer cation could occupy several kinds of coordination sites between the NbO_6 and TiO_6 octahedral layers, depending on its size and its electric charge [28]. A larger cation, such as aqueous Mn^{2+} or Ni^{2+}, is located at a larger polyhedral site, interacting with more Nb–O bonds than K^+. It could be another reason to the blue shift of the IR vibration absorption peak [29]. This effect to the bond vibration could be consistent with one caused by electrostatic interaction.

3.4. UV–vis diffuse reflection spectra

Fig. 7 shows the UV–vis diffuse reflectance spectra of the samples and the first derivatives patterns of the samples respectively. Additionally, the band energy gaps (E_g) of all

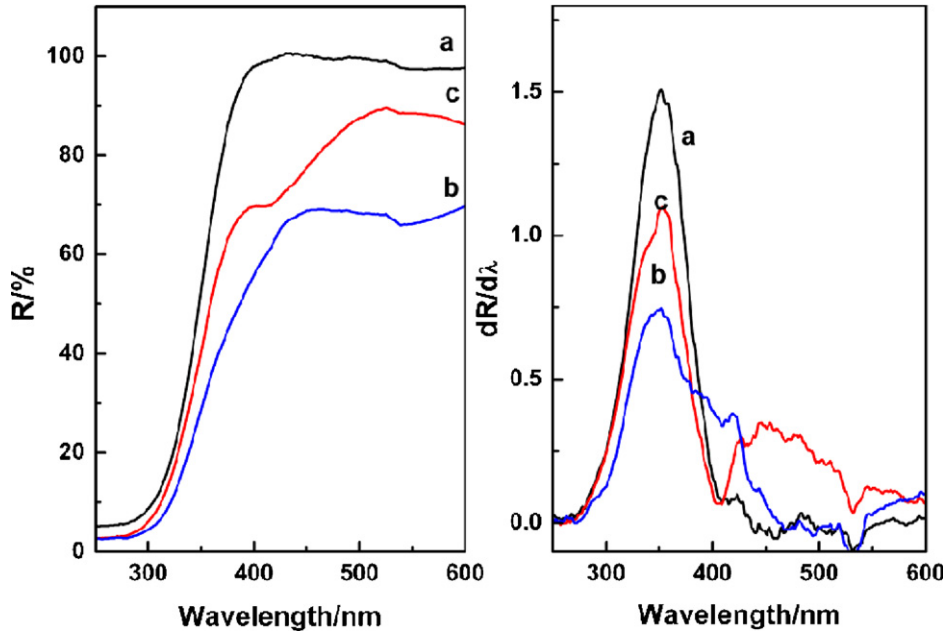

Fig. 7. UV–vis DRS of the catalysts: (a) $KTiNbO_5$; (b) $K_{1-2x}Mn_xTiNbO_5$; and (c) $K_{1-2x}Ni_xTiNbO_5$.

Table 1
The band energy gap values of the samples as-prepared.

Sample	λ_{max1} (nm)	E_{g1} (eV)	λ_{max2} (nm)	E_{g2} (eV)
$KTiNbO_5$	351	3.53	–	–
$K_{1-2x}Mn_xTiNbO_5$	351	3.53	419	2.96
$K_{1-2x}Ni_xTiNbO_5$	353	3.51	468	2.65

investigated samples as-prepared calculated from the Planck equation have been summarized in Table 1.

As shown in Fig. 7, the reflectance spectra of the samples vary strongly according to the interlayer cationic species. For host $KTiNbO_5$ (spectrum Fig. 7(a)), the absorption edge is 351 nm (E_g = 3.91 eV), which indicates that host layered $KTiNbO_5$ absorbs UV light only. Whereas in the case of $K_{1-2x}Mn_xTiNbO_5$, and $K_{1-2x}Ni_xTiNbO_5$ (spectra Fig. 7(b) and (c), respectively), one can notice that the reflection intensity decreased from that of $KTiNbO_5$, and a new absorption edge (λ_{max} = 419 nm, or 468 nm for $K_{1-2x}Mn_xTiNbO_5$ or $K_{1-2x}Ni_xTiNbO_5$, respectively) in the visible light region can be observed. The presence of this additional absorption edge could be caused by Mn^{2+} or Ni^{2+} ion, which replaces K^+ ion through ion-exchange due to the electric translation from Mn^{2+} or Ni^{2+} ion to titanoniobate sheets.

Factors affecting the band energy gaps of layered compounds with interlayer cations are considered as follows [30]. (1) The interaction between layers. As the ionic radius of cations at the interlayer becomes large, the distance between layers becomes larger; accordingly an excited energy state becomes localized by decreasing interaction between the layered. (2) The polarization ability of cations at the interlayer towards the oxygen ions of octahedral faced at the interlayer. In short, it can be suggested that there exist interaction between the interlayer cations and terminal Nb–O bond, which has been confirmed by FT-IR, as shown in Fig. 6.

For $K_{1-2x}Mn_xTiNbO_5$ or $K_{1-2x}Ni_xTiNbO_5$, another key feature, Mn^{2+} or Ni^{2+} 3*d* electrons provide these new band gap levels, which reduce the band gap energy of the material and cause a red shift in its photoabsorption edge. As a result, *d*-electron metal intercalation improves the photoabsorption of $KTiNbO_5$, and which enrich the exchanged samples with photocatalytic activity under visible light radiation.

3.5. Adsorption feature and photocatalytic oxidation characteristics of methyl mercaptan

FT-IR spectroscopy is useful to determine surface adsorbed species responsible for the reaction process and catalyst deactivation. The adsorption feature and photocatalytic oxidation activity for MM in methane are evaluated through the vibration spectra of species on the samples disclosed by FT-IR. Figs. 8 and 9 show these spectra in the 2000–1000 cm^{-1} range.

For $KTiNbO_5$, its FT-IR spectrum was represented in Fig. 8(a). All of the absorption bands corresponding to the C–H stretching vibration, C–S wagging vibration and C–S stretching vibration are not observed. The result indicates that there is a weak interaction between MM and $KTiNbO_5$, thus MM or any its dissociated product was not adsorbed on the host $KTiNbO_5$

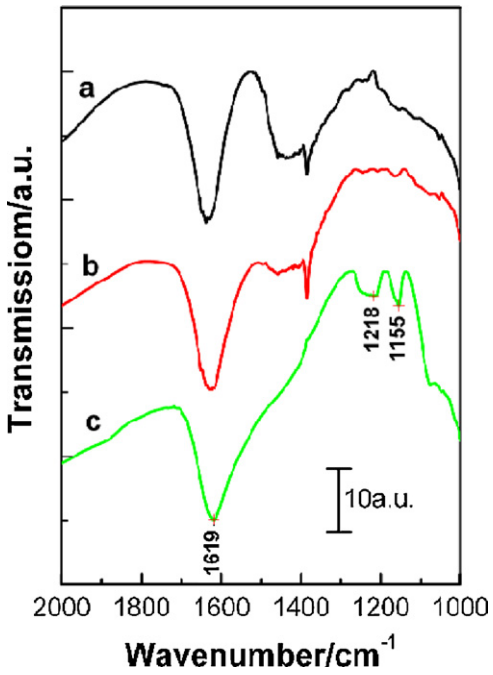

Fig. 8. IR spectra of the $K_{1-2x}M_xTiNbO_5$ (M = Mn, Ni) after MM in methane adsorption under visible light: (a) $KTiNbO_5$; (b) $K_{1-2x}Mn_xTiNbO_5$; and (c) $K_{1-2x}Ni_xTiNbO_5$.

under visible light. However, when the adsorption process was carried out under ultraviolet light irradiating, a new absorption band observed at ~1115 cm^{-1} corresponds to the S=O stretching vibration [31,32] in HO–SO_2–R (sulfonic acids), which could be the product of MM photocatalytic oxidization by $KTiNbO_5$ under ultraviolet light irradiating. The result was consistent with that the only UV absorbance of the as-prepared $KTiNbO_5$.

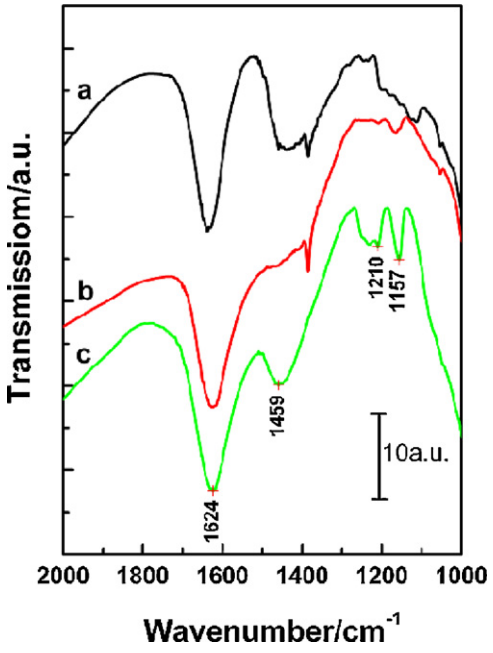

Fig. 9. FT-IR spectra of the $K_{1-2x}M_xTiNbO_5$ (M = Mn, Ni) after MM in methane photocatalytic oxidation under UV light radiation: (a) $KTiNbO_5$; (b) $K_{1-2x}Mn_xTiNbO_5$; and (c) $K_{1-2x}Ni_xTiNbO_5$.

In regard to $K_{1-2x}Mn_xTiNbO_5$, when the adsorption process is under visible or ultraviolet light irradiating, there is an absorption band at ~1164 cm^{-1} which is observed in both spectrum Figs. 8(b) and 9(b). According to the FT-IR spectra, the only final product of the MM photocatalytic oxidation on the $K_{1-2x}Mn_xTiNbO_5$ was sulfonic acid. However, for $K_{1-2x}Ni_xTiNbO_5$, when the adsorption process was carried out under visible light, there were two characteristic absorbance bands as shown in spectrum Fig. 8(c). The band at ~1115 cm^{-1} could be attributed to the S=O stretching vibration [32] in HO–SO_2–R (sulfonic acids), and the band at the range of 1210–1240 cm^{-1} could arise from the surface bidentate carbonates [33]. The latter may be induced by the C–S bond (methyl mercaptan) cleavage and the carbon atom oxidation under visible light radiation comparing to spectrum Fig. 8(c), the spectrum Fig. 9(c) has a new intensive band at 1459 cm^{-1} which can be attributed to surface carboxylate.

For photocatalytic oxidation of MM, several organic intermediates were detected on the samples. Then, it could be suggested that three different types of reaction happened at the process of light irradiation as following. The first process is the oxidation for sulfur, the second process is the oxidation of carbon, and the third process is the cleavage and oxidation of C–S bond. In all cases, the S atoms in the sulfides were oxidized. However, whether C–S bond broken or C atom oxidized depended on interlayer cations of the titanoniobates as well as radiation-light wavelength.

4. Conclusions

In this paper, hydrothermal synthesis process has been used to synthesize the layered $KTiNbO_5$ with the higher surface area. The ion exchange with Mn^{2+} and Ni^{2+} has produced novel photocatalytic materials. The results showed that the absorption band of $K_{1-2x}M_xTiNbO_5$ (M = Mn, Ni) had shifted from UV region to visible region for the interaction between the interlayer cations and Nb–O band and their *d*-electron providing new band gap levels. Meanwhile, $K_{1-2x}Mn_xTiNbO_5$ $TiNbO_5$ and $K_{1-2x}Ni_xTiNbO_5$ show activities towards photocatalytic oxidation of MM in methane under visible light and UV-light radiation. The surface adsorbed species disclosed by FT-IR spectra demonstrated that the different interlayer cations could change the reaction path during photocatalytic oxidization process of MM.

Acknowledgements

The authors acknowledge the financial supports from Natural Science Foundation of China (21071004) and Natural Science Foundation of Anhui Province of China (11040606M38).

References

[1] A.V. Vorontsov, E.V. Savinov, L. Davydov, et al., Photocatalytic destruction of gaseous diethyl sulfide over TiO_2, Appl. Catal. B: Environ. 32 (2001) 11–24.

[2] K. Demeestere, J. Dewulf, B. De Witte, et al., Titanium dioxide mediated heterogeneous photocatalytic degradation of gaseous dimethyl sulfide: parameter study and reaction pathways, Appl. Catal. B: Environ. 60 (2005) 93–106.

[3] X.Z. Li, M.F. Hou, F.B. Li, et al., Photocatalytic oxidation of methyl mercaptan in foul gas for odor control, Ind. Eng. Chem. Res. 45 (2006) 487–494.

[4] N. Gonzalez-Garcia, J.A. Ayllon, X. Domenech, et al., TiO_2 deactivation during the gas-phase photocatalytic oxidation of dimethyl sufide, Appl. Catal. B: Environ. 52 (2004) 69–77.

[5] J. He, J.B. Zhao, Y.X. Lan, Adsorption and photocatalytic oxidation of dimethyl sulfide and ethyl mercaptan over layered $K_{1-2x}Mn_xTiNbO_5$ and $K_{1-2x}Ni_xTiNbO_5$, J. Fuel Chem. Technol. 37 (2009) 485–488.

[6] K. Inoue, S. Suzuki, M. Nagai, Ion exchanged potassium titanoniobate as photocatalyst under visible light, J. Electroceram. 24 (2010) 10–114.

[7] Z.W. Tong, S. Takagi, T. Shimada, et al., Photoresponsive multilayer spiral nanotubes: intercalation of polyfluorinated cationic azobenzene surfactant into potassium niobate, J. Am. Chem. Soc. 128 (2006) 684–685.

[8] A. Kudo, E. Kaneko, Photoluminesent properties of ion-exchangeable layered oxides, Micropor. Mesopor. Mater. 21 (1998) 615–620.

[9] T. Nakato, K. Kusunoki, K. Yoshizawa, Photoluminescence of tris(2,2′-bipyridine) uthenium(II) ions intercalated in layered niobates and titanates: effect of interlayer structure on host–guest and guest–guest interactions, J. Phys. Chem. 99 (1995) 17896–17905.

[10] C.C. Owen, E.O. Frank, Niobate nanosheets as catalysts for photochemical water splitting into hydrogen and hydrogen peroxide, J. Phys. Chem. C 113 (2009) 479–485.

[11] Y.N. Guo, L. Chen, F.Y. Ma, et al., Efficient degradation of tetrabromobisphenol A by heterostructured $Ag/Bi_5Nb_3O_{15}$ material under the simulated sunlight irradiation, J. Hazard. Mater. 189 (2011) 614–618.

[12] C. Zhou, G. Chen, Q. Wang, High photocatalytic activity of porous $K_4Nb_6O_{17}$ microsphere with large surface area prepared by homogeneous precipitation using urea, J. Mol. Catal. A: Chem. 339 (2011) 7–42.

[13] E. Yasuo, S. Nobuyuki, S. Takayoshi, Photocatalyst of lamellar aggregates of RuOx-loaded perovskite nanosheets for overall water splitting, J. Phys. Chem. B 109 (2005) 17212–17216.

[14] B. Li, Y. Hakuta, H. Hayashi, Synthesis of potassium titanoniobate in supercritical and subcritical water and investigations on its photocatalytic performance, J. Supercrit. Fluids 39 (2006) 63–69.

[15] A.S. Dias, S. Lima, D. Carriazo, et al., Exfoliated titanate, niobate and titanoniobate nanosheets as solid acid catalysts for the liquid-phase dehydration of D-xylose into furfural, J. Catal. 244 (2006) 30–237.

[16] J.S. Jang, H.G. Kim, V.R. Reddy, et al., Photocatalytic water splitting over iron oxide anoparticles intercalated in $HTiNb(Ta)O_5$ layered compounds, J. Catal. 231 (2005) 13–222.

[17] G.K. Zhang, F.S. He, X. Zou, et al., Hydrothermal preparation and photocatalytic properties of sheet-like nanometer niobate $K_4Nb_6O_{17}$, J. Phys. Chem. Solids 69 (2008) 471–1474.

[18] H. Takahshi, M. Kakihana, Y. Yamashita, et al., Synthesis of NiO-loaded $KTiNbO_5$ photocatalysts by a novel polymerizable complex method, J. Alloys Compd. 285 (1999) 77–81.

[19] A. Kudo, Y. Miseki, Heterogeneous photocatalyst materials for water splitting, Chem. Soc. Rev. 38 (2009) 253–278.

[20] H. Takahashi, M. Kakihana, Y. Yamashita, et al., Synthesis of $(H_3O)TiNbO_5{\cdot}0.26H_2O$ via hydronium (H_3O^+) ion-exchange reaction and its photocatalytic activity for H_2 evolution from aqueous methanol solution, Phys. Chem. Chem. Phys. 2 (2000) 4461–4464.

[21] C. Tagusagawa, A. Takagaki, S. Hayashi, et al., Characterization of $HNbWO_6$ and $HTaWO_6$ metal oxide nanosheet aggregates as solid acid catalysts, J. Phys. Chem. C 113 (2009) 7831–7837.

[22] Y. Hosogi, H. Kato, A. Kudo, Photocatalytic activities of layered titanates and niobates ion-exchanged with Sn^{2+} under visible light irradiation, J. Phys. Chem. C 112 (2008) 7678–17682.

[23] Q.Q. Wang, B.Z. Lin, B.H. Xu, et al., Preparation and photocatalytic properties of mesoporous SnO_2-hexaniobate layered nanocomposite, Micropor. Mesopor. Mater. 130 (2010) 344–351.

[24] L.D. Arsov, C. Kormann, W. Plieth, Electrochemical synthesis and in situ Raman spectroscopy of thin films of titanium dioxide, Raman Spectrosc. 22 (1991) 573–575.
[25] Z. Zhang, J.B.M. Goodall, S. Brown, et al., Continuous hydrothermal synthesis of extensive 2D sodium titanate ($Na_2Ti_3O_7$) nano-sheets, Dalton Trans. 39 (2010) 711–714.
[26] D. Prasetyoko, Z. Ramli, S. Endud, et al., Preparation and characterization of bifunctional oxidative and acidic catalysts Nb_2O_5/TS-1 for synthesis of diols, Mater. Chem. Phys. 93 (2005) 443–449.
[27] E. Da Costa, C.O. Avellaneda, A. Pawlicka, Alternative Nb_2O_5–TiO_2 thin films for electrochromic devices, J. Mater. Sci. 36 (2001) 1407–1410.
[28] S.H. Byeon, H. Nam, Neutron diffraction and FT-Raman study of ion-exchangeable layered titanates and niobates, J. Chem. Mater. 12 (2000) 1771.
[29] K. Saruwatari, H. Sato, T. Idei, et al., Photoconductive properties of organic–inorganic hybrid films of layered perovskite-type niobate, J. Phys. Chem. B 109 (2005) 12410–12416.
[30] Y. Miseki, H. Kato, A. Kudo, Water splitting into H_2 and O_2 over niobate and titanate photocatalysts with (1 1 1) plane-type layered perovskite structure, Energy Environ. Sci. 2 (2009) 306–314.
[31] J.G. Wu, Technology, Application of Modern FTIR Spectroscopy [M], Science and Technology Literature Press, Beijing, 1994.
[32] The Sadtler Handbook of Infrared Spectra [M]. Bio-Rad Laboratories Inc., Informatics Division, 2004, pp. 85–95.
[33] D.V. Kozlov, A.V. Vorontsov, P.G. Smirniotis, et al., Gas-phase photocatalytic oxidation of diethyl sulfide over TiO_2: kinetic investigations and catalyst deactivation, Appl. Catal. B: Environ. 42 (2003) 77–87.